INL/CON-22-67990-Revision-0

Analytical homogenization techniques applied to the Fickian diffusion: Effective diffusivity coefficient

November 2022

Aysenur Toptan, Wen Jiang, Jason D Hales

Changing the World's Energy Future

Idaho National Laboratory

INL is a U.S. Department of Energy National Laboratory operated by Battelle Energy Alliance, LLC

INL/CON-22-67990-Revision-0

Analytical homogenization techniques applied to the Fickian diffusion: Effective diffusivity coefficient

Aysenur Toptan, Wen Jiang, Jason D Hales

November 2022

Idaho National Laboratory
Idaho Falls, Idaho 83415

http://www.inl.gov

Prepared for the
U.S. Department of Energy
Under DOE Idaho Operations Office
Contract DE-AC07-05ID14517

Analytical homogenization techniques applied to the Fickian diffusion: Effective diffusivity coefficient

Aysenur Toptan*,†, Wen Jiang†, and Jason D. Hales†

†*Computational Mechanics & Materials, Idaho National Laboratory, P.O. Box 1625, Idaho Falls, ID United States*
**aysenur.toptan@inl.gov*

INTRODUCTION

For multiple applications in nuclear energy, the ability to accurately represent material behavior with a simplified model is important to facilitate practical engineering-scale simulations. In this work, we focus on the homogenized thermal response of a medium containing spherical inclusions, similar to a fuel form (compact or pebble) containing tri-structural isotropic (TRISO) particles. An extensive survey on effective thermal conductivity (ETC) modeling was performed in our previous study [1], considering a random distribution of mono-sized spherical inclusions in a continuous matrix.

The governing equations of elasticity, thermal conduction, and electrical conduction problems in the steady state have similar mathematical forms (Table I). Most approaches developed for conductive problems can be extended to corresponding elastic problems, as well as to the simplified Fickian diffusion that is widely used for the conservative calculations in engineering applications. Using the analogy between heat conduction (see Eq. 1) and the simplified Fickian diffusion (or fission product species conservation, see Eq. 2), we can use the same analytical homogenization methods to obtain ETC as for the effective diffusivity coefficient (EDC). Based on our previous work for the ETC in [1, 2], the effective medium theory (EMT) showed the best agreement for $\alpha > 1$ while differential EMT (D-EMT) for $\alpha < 1$ where α is defined as the ratio of thermal conductivities of particles to continuous medium for the ETC calculations. In this study, we selected only the recommended these two ETC models (see Table II) to see if our hypothesis is valid for EDC calculations.

The heat conduction is given by:

$$\rho c_P \frac{\partial T}{\partial t} - \nabla \cdot (k \nabla T) - q''' = 0 \tag{1}$$

where T is temperature and it varies in time t and space $\boldsymbol{x}$, as determined by the definition of the differential operator ∇ for a given coordinate system. Here, ρ, c_P, and k are density, specific heat, and thermal conductivity, respectively, and q''' is the volumetric source rate.

Fission product species conservation is given by:

$$\frac{\partial C}{\partial t} + \nabla \cdot \boldsymbol{J} + \lambda C - S = 0 \tag{2}$$

where C is concentration, λ and S are the radioactive decay constant and source rate of a given species; and $\boldsymbol{J}$ is the mass flux. Radioactive decay is often neglected (i.e., $\lambda = 0$). The mass flux is:

$$\boldsymbol{J} = -D \nabla C \tag{3}$$

using the diffusion coefficient, D (m^2/s) that is defined in a temperature-dependent Arrhenius form as:

$$D = \sum_i D_{0,i} \exp\left(-\frac{Q_i}{RT}\right) \tag{4}$$

where R is the universal gas constant.

We performed several numerical experiments using the finite-element based code Bison[1] [6] and assess the recommended analytical models for EDC. These numerical experiments are conducted for a domain with randomly dispersed, mono-sized spherical particles with varying material properties.

METHODS

The methodology is described to obtain in three main steps the EDC from the FEAs and the problem settings in each from the converged concentration profile for the effective diffusivity coefficient.

Step 1. We create a 3-D cubic computational domain of a representative volume element of material with randomly dispersed, mono-sized spheres in Fig. 1. The spheres are described by a field variable in a diffuse manner. This field variable equals one within the spheres and varies continuously, but steeply, to zero within the secondary phase. The diffusive interface width is a user-controlled parameter, and is set to 10% of the sphere diameter here. The adaptive meshing is utilized to resolve the phase interface by using two levels of refinement in the regions on the periphery of each sphere. The distance between centers of two adjacent spheres, d, is required to be at least one sphere diameter, D, so that there is no overlap between the spheres (i.e., $d \geq d_{\min} = 1.05D$).

Step 2. Finite element analysis (FEA) simulations are performed for different volume fractions in each numerical experiment. Different volume fractions are obtained via varying the number of spheres in the computational domain. In this study, we consider the evaluation of EDC; therefore, only Eq. 2 is solved. The diffusivity coefficients of both the host matrix and the spherical inclusions are chosen based on the analyses of interest. The diffusivity coefficient is weighted based on the volume fraction of each phase for a cell including both phases. The numerical simulations are performed up to approximately 40% packing fraction.

Step 3. The EDC is calculated from the converged concentration field using the relation from [7] as:

$$D_{e,x} = \frac{\int_A \int D_b \left(\frac{\partial C}{\partial x}\right)_{x=L} dydz}{\frac{(C_2 - C_1)}{L} A} \tag{5}$$

where D_b is the bulk diffusivity coefficient (or matrix diffusivity coefficient), C_1 and C_2 are the concentration values applied to each opposing surface in the unidirectional diffusion process, and A is the surface area. To obtain a single value for

[1]Though MOOSE is open source, Bison is export controlled. Institutional access can be requested through Idaho National Laboratory's Nuclear Computational Resource Center (`https://inl.gov/ncrc/`).

TABLE I: Correspondence between elastic and conductive problems, taken from [3].

Problem	**Elasticity**	**Thermal Conductance**	**Electric Conductance**
Corresponding quantities	Stress $\boldsymbol{\tau}$	Heat flux $\boldsymbol{q}$	Current $\boldsymbol{J}$
	Displacement $\boldsymbol{u}$	Temperature T	Electrical potential ϕ
	Strain $\boldsymbol{\epsilon} = \frac{1}{2}(\nabla \boldsymbol{u} + (\nabla \boldsymbol{u})^{\intercal})$	Thermal gradient $\boldsymbol{g} = -\nabla T$	Electric field intensity $\boldsymbol{E} = -\nabla \phi$
	Elasticity tensor $\mathbb{C}$	Thermal conductivity tensor $\boldsymbol{K}$	Electric conductivity tensor $\boldsymbol{\sigma}$
Equilibrium eq.	$\nabla \cdot \boldsymbol{\tau} = 0$	$\nabla \cdot \boldsymbol{q} = 0$	$\nabla \cdot \boldsymbol{J} = 0$
Physical eq.	$\boldsymbol{\tau} = \mathbb{C} : \epsilon$	$\boldsymbol{q} = \boldsymbol{K} \cdot \boldsymbol{g}$	$\boldsymbol{J} = \boldsymbol{\sigma} \cdot \boldsymbol{E}$

TABLE II: Recommended analytical methods for the ETC based on our previous work in [1, 2]. The nomenclature: k_e is the ETC, k_1 and υ_1 are the thermal conductivity and volume fraction of continuous phase, k_2 and υ_2 are the thermal conductivity and volume fraction of dispersed phase, and $\alpha = k_2/k_1$ is the ratio of the thermal conductivities of dispersed phase to continuous phase.

	Model	**Formulation**	**Notes**
$\alpha < 1$	D-EMT	$\left(\frac{k_e - k_2}{k_1 - k_2}\right)^3 \frac{k_1}{k_e} = (1 - \upsilon_2)^3$	Roots of the 3rd-order polynomial are computed accordingly and the largest real root of the cubic equation is assigned to the ETC [4].
$\alpha > 1$	EMT	$\sum_i \upsilon_i \left(\frac{k_i - k_e}{k_i + 2k_e}\right) = 0$	The *Bruggeman* [5] obtained the following relation for a binary system: $\frac{k_e}{k_1} = \alpha A + \sqrt{\alpha^2 A^2 + \frac{\alpha}{2}}$ with $A = \frac{1}{4}\left(3\upsilon_2 - 1 + \frac{1}{\alpha}[2 - 3\upsilon_2]\right)$

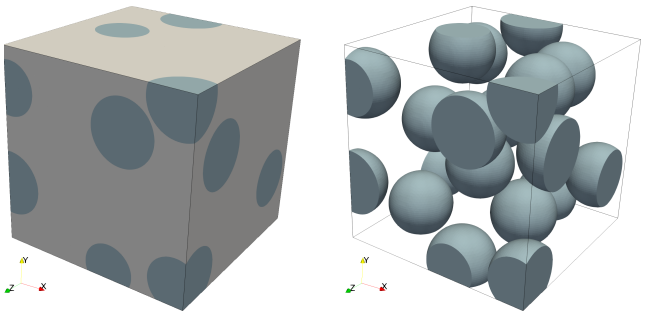

(a) (b)

Fig. 1: 3-D constructed computational domain: (a) Matrix with embedded spheres. (b) Random distribution of mono-sized spheres (matrix is hidden for ease of visibility). The characteristic domain length-to-particle radius, L/R is 6. The volume fraction of the continuous matrix, υ_1 is 0.726. The minimum distance between centers of two adjacent spheres is set to one sphere diameter D (i.e., $d_{\min} = D$).

EDC from the set of simulations, an arithmetic mean of the diffusivity coefficients in the principal directions is employed as:

$$D_e = \frac{1}{n}\left(\sum_{i=1}^{n} D_{e,i}\right) \tag{6}$$

where $D_{e,i}$ represents the diffusivity coefficient in each principal direction (via Eq. 5) and n is the number of principal directions (i.e., $n = 3$ for 3-D).

RESULTS & DISCUSSION

The FEAs are performed for the computational domain at various volume fractions. The EDC is evaluated for randomly dispersed mono-sized spherical inclusions embedded in a continuous matrix considering two cases: (1) diffusivity coefficient of the particles is less than the continuous matrix ($\alpha = D_2/D_1 < 1$), and (2) diffusivity coefficient of the particles are greater than the continuous matrix ($\alpha > 1$). The details of the results are provided and discussed. Note that $\alpha = 1$ corresponds to the homogeneous material; therefore, it is not evaluated here.

The simulation results and model predictions are provided in terms of the diffusivity coefficients ratio of the effective to host matrix, D_e/D_1, to understand the impact of spherical inclusions with varying diffusivity coefficients, as a function of the volume fraction of matrix, υ_1. The characteristic domain length-to-particle, L/R is set to 6 in these analyses for the computational considerations, which is found to be sufficient from the parametric study performed in [1, 2]. Only uncertainty around the mean FEA results vary with the chosen L/R ratio, which are indicated with the error bars around the FEA predictions.

Case I. Diffusivity coefficient of the particles is less than the continuous matrix ($\alpha < 1$).

Fig. 2 shows the concentration profiles for the case with $\alpha < 1$ in each unidirectional diffusion process in the principal direction at a fixed volume fraction of the continuous matrix, υ_1 of 0.726 for arbitrarily chosen α =1×10^{-4}, 0.1, and 0.5.

See Fig. 1 for the actual particle locations with υ_1 =0.726. The FEA-predicted D_e is estimated from the average values of realizations performed in all three principal directions, which are plotted in Fig. 3 as well as the model predictions from both EMT and D-EMT. In this case, the diffusion gradient across the domain is relatively smooth at α = 0.5 (see Fig. 2c). The presence of the particles within the domain becomes more pronounced on the diffusion process as α approaches zero (see Fig. 2a and Fig. 2b).

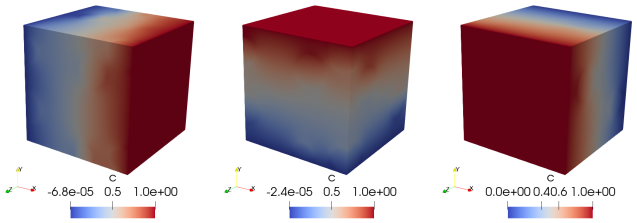

(a) α =1×10^{-4}

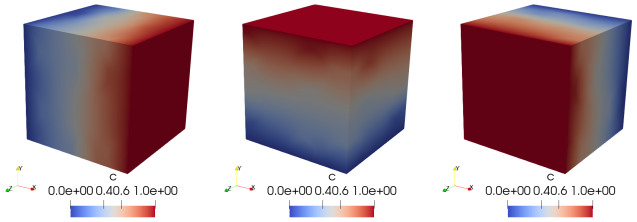

(b) α =0.1

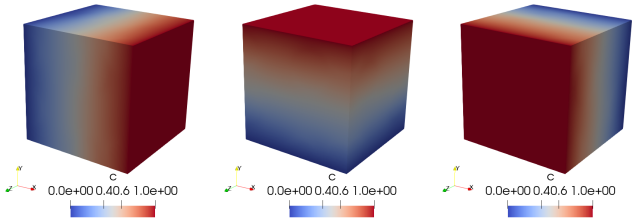

(c) α =0.5

Fig. 2: Concentration profile contours obtained from the unidirectional diffusion process in x-, y-, and z-direction at fixed υ_1 =0.726 (see Fig. 1 for the actual particle locations) for (a) α =1×10^{-4}, (b) α =0.1, and (c) α =0.5. The FEA-predicted D_e is estimated from the average of three realizations performed in each principal direction.

Fig. 3 shows the model and FEA predictions of D_e/D_1 as a function of υ_1 for arbitrarily chosen α=1×10^{-4}, 0.1, and 0.5. As expected, the inclusion of less diffusive particles to the system degrades the overall diffusivity coefficient of system. As expected, the material behaves as a homogeneous material at υ_1 = 1. The models behave similar for α = 0.5, while significantly differentiate from each as α becomes smaller. As suggested in Ref. [1], the D-EMT represents the expected behavior well for α < 1 in the estimation of EDC. The numerical simulations are performed up to approximately 40% packing. The maximum packing fraction for different arrangements—e.g., face-centered cubic (FCC), hexagonal close (HC), random close/loose, and simple cubic (SC)—are indicated in Fig. 3 [8].

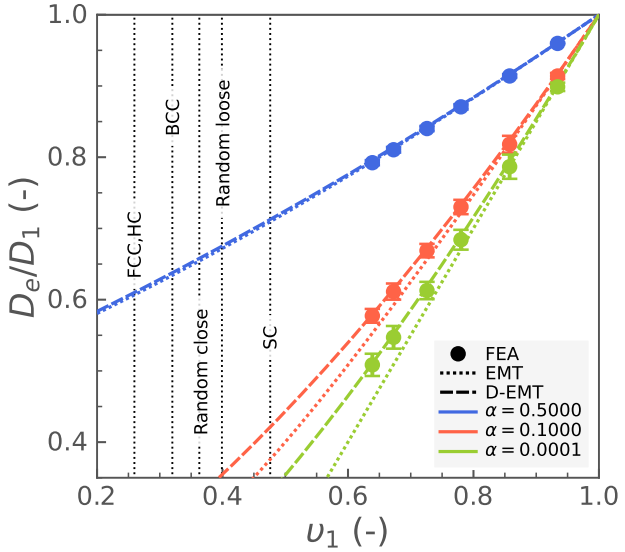

Fig. 3: D_e/D_1 predictions with respect to υ_1 at α =1×10^{-4}, 0.1, and 0.5. The model-predicted D_e/D_1 values are plotted against the expected FEA predictions. The packing fraction, υ_2 can be obtained from $1-\upsilon_1$ in a binary system. The dashed lines represent the maximum packing fractions for different arrangements (e.g., FCC, HC, random close/loose, and SC).

Case II. Diffusivity coefficient of the particles is greater than the continuous matrix (α > 1).

Fig. 4 shows the concentration profiles for the case with α > 1 this time. Similarly, the unidirectional diffusion process is illustrated in each principal direction at fixed υ_1 =0.726 for arbitrarily chosen α =2.0, 10.0, and 100.0. See Fig. 1 for the actual particle locations at υ_1 =0.726.

The FEA and model predictions of D_e/D_1 are plotted in Fig. 5 as a function of υ_1 at the selected α values. The inclusion of more diffusive particles to the medium increases the overall diffusivity coefficient of system. The models behave similar only up to 10% packing fraction (i.e., $\upsilon_2 = 1-\upsilon_1 = 0.10$) and significantly vary from each other as more particles are present in the system at higher α values. As suggested in Ref. [1] for the ETC, the EMT represents the expected behavior relatively better for α > 1 in the estimation of EDC.

CONCLUSIONS

The analytical methods for the ETC of a medium with spherical inclusions is investigated previously in Ref. [1]. Although the focus of previous study was on the macroscopic description of thermal conductivity, similar discussions and conclusions are valid for diffusivity coefficients due to having similar mathematical forms. In this study, we extended our studies and examined the validity of models for the effective diffusivity calculations, obtained from the Fickian diffu-

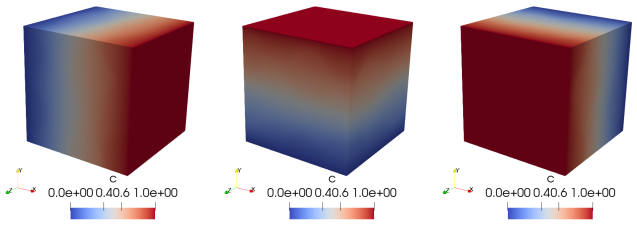

(a) α =2.0

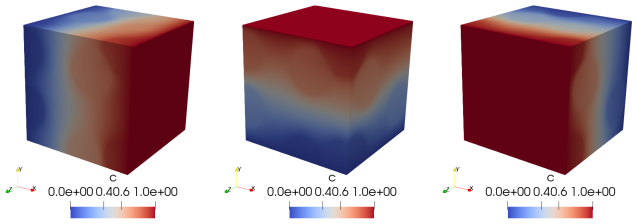

(b) α =10.0

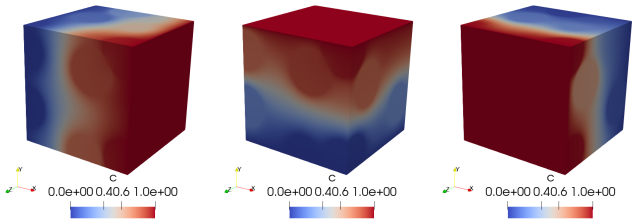

(c) α =100.0

Fig. 4: Concentration profile contours obtained from the unidirectional diffusion process in x-, y-, and z-direction at fixed υ_1 =0.726 (see Fig. 1 for the actual particle locations) for (a) α =2.0, (b) α =10.0, and (c) α =100.0. The FEA-predicted D_e is estimated from the average of three realizations performed in each principal direction.

sion. The models that we examined in our earlier study [1, 2] (D-EMT for $\alpha < 1$ and EMT for $\alpha < 1$) were only taken into the consideration in this study. Each analytical model was evaluated with respect to the expected EDC obtained from the FEA simulations under a variety of conditions. The FEA simulations were performed up to approximately 40% packing in our analyses. We observed similar model behaviors from each model for the EDC estimation of a binary system: D-EMT for $\alpha < 1$ and EMT for $\alpha > 1$ where α is defined as the ratio of the diffusivity coefficient of spheres to that of the host matrix. These numerical results establish the regimes where these analytical formulations can be used with high confidence for applications of interest, particularly for the estimation of EDC from the Fickian diffusion for the TRISO applications. Both EMT and D-EMT approaches, among many others detailed in Ref. [1], are available in the Bison code.

ACKNOWLEDGMENTS

The partnership of Kairos Power, LLC, including contributions to the source code and documentation for TRISO capabilities, is gratefully acknowledged.

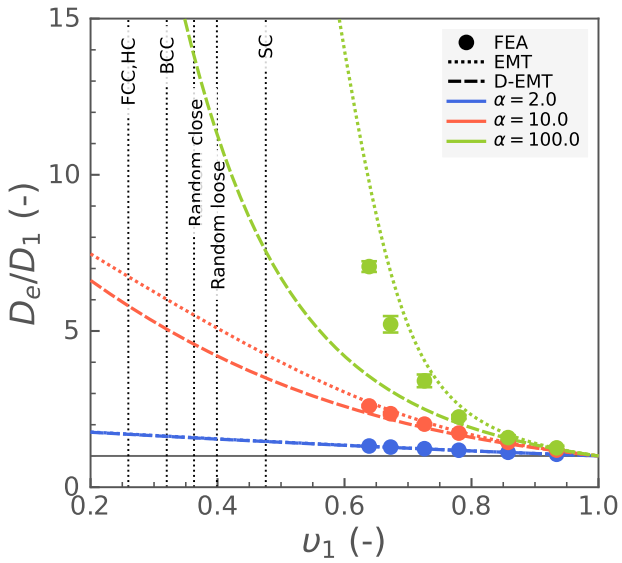

Fig. 5: D_e/D_1 predictions with respect to υ_1 at α =2.0, 10.0, and 100.0. The model predictions and regions determined by upper and lower bounds of the D_e/D_1 predictions are plotted against the expected FEA predictions. The packing fraction, υ_2 can be obtained from $1 - \upsilon_1$ in a binary system. The dashed lines represent the maximum packing fractions for different arrangements (e.g., FCC, HC, random close/loose, and SC).

REFERENCES

1. A. TOPTAN, W. JIANG, J. D. HALES, ET AL., *Nucl. Eng. Des.*, **381**, 111355 (2021).
2. W. JIANG, A. TOPTAN, J. D. HALES, ET AL., Tech. Rep. INL/EXT-21-63549, INL, United States (6 2021).
3. F. DENG and Q. ZHENG, *Acta Mech. Solida Sin.*, **22**, *1*, 1–17 (2009).
4. A. TOPTAN, D. J. KROPACZEK, and M. N. AVRAMOVA, *Nucl. Eng. Des.*, **350**, 1–8 (2019).
5. D. BRUGGEMAN, *Ann. Phys. (Leipzig)*, **24**, 636–664 (1935).
6. R. L. WILLIAMSON, J. D. HALES, S. R. NOVASCONE, ET AL., *Nucl Technol.*, **207**, *7*, 954–980 (2021).
7. D. MU, Z. LIU, C. HAUNG, ET AL., *J. Porous Mater.*, **14**, 49–54 (2007).
8. L. E. NIELSEN, *Ind. Eng. Chem. Fundam.*, **13**, *1*, 17–20 (1974).